JOURNAL OF MATERIALS SCIENCE 16 (1981) 1579–1591

Erosion of MgO by solid particle impingement at normal incidence

D. G. RICKERBY, N. H. MACMILLAN
Materials Research Laboratory, The Pennsylvania State University, University Park, Pennsylvania 16802, USA

A study has been made of the erosion of almost fully dense, fine-grained MgO by millimeter-scale WC–6 wt% Co spheres impinging at normal incidence with velocities between 10 and 90 m sec^{-1}. Scanning electron microscopy showed that the damage consisted of a central crater surrounded by an array of intergranular radial and/or median and/or lateral cracks characteristic of an elastic–plastic impact. The crater had a thin lining of plastically deformed material, but appeared to have been formed primarily by localized transgranular and integranular fracture processes, suggesting that any mode of irreversible deformation in the contact region will suffice to produce the changeover from Hertzian cracking to radial, median and lateral cracking. The accompanying gravimetric studies showed that mass loss, which was caused primarily by intersection of lateral cracks with the free surface and with radial and/or median cracks, increased threefold during the short incubation period in which the as-received surface evolved into its steady-state eroded condition. During this period the exponent relating erosion to impact velocity decreased asymptotically towards a value smaller than that predicted by any current theory of erosion in the elastic or the elastic–plastic impact regime. Nor are these theories any more successful at explaining the observed particle-size dependence of the erosion of polycrystalline MgO.

1. Introduction

Until recently, understanding of the erosion of ceramics by solid particle impingement (reviewed in [1] and [2]) was based largely on the work of Finnie and co-workers [3–7]. Starting from the assumption that ceramics behave in a totally brittle manner, these authors combined Hertz's [8] or Hamilton and Goodman's [9] analysis of the stress arising from static elastic contact between a sphere and a half-space with Weibull's probabilistic treatment of fracture [10] to obtain an estimate of the amount of material removed by a typical normal or oblique impact, respectively. The resultant model is only semi-quantitative, but it provides a satisfactory rationalization of the many different empirical relationships between erosion and particle size or particle velocity that have been reported. It also predicts quite well the observed angular dependence of the erosion of brittle materials and provides a convincing explanation of their tendency to erode in an increasingly ductile manner as the size of the erosive particles is reduced [11, 12]. An essentially similar model has recently been proposed by Sargent *et al.* [13].

During the last decade, however, it has become widely recognized that many ceramics exhibit some plasticity in response to "sharp" contact loading, and that this plasticity exerts a significant effect on the nature and extent of the cracking that takes place in and around the region of contact. In particular, plastic flow beneath a normally loaded hard indenter or a hard particle impacting at normal incidence tends to suppress the formation of Hertzian cone cracks and promote instead the creation of various characteristic combinations of lateral, radial, median and cone* cracks about the plastic zone. The formation of such arrays

* These cone cracks are distinguished from the Hertzian cone cracks formed in a purely elastic contact because their different inclination to the specimen surface suggests that plastic deformation was involved in their formation.

0022–2461/81/061579–13$03.30/0

during static indentation has been studied in hardened steel [14], WC–Co cermets [15–18], polymethyl-methacrylate [19–21], solid high explosives [22], Ge [23, 24], Si [24, 25], SiC [24, 26–28], Al_2O_3 [24, 27, 29–31], LiF [32], NaCl [24, 31], ZnS [31], ZnSe [31], quartz [25], a spinel [31], Si_3N_4 [31], various rocks [33, 34], fused SiO_2 [25] and a wide variety of silicate glasses [25, 31, 35–45]. In addition, numerous attempts have been made to understand the deformation processes involved in the nucleation of these cracks [24, 39, 43, 46, 47], the fracture mechanics of their propagation [18, 20, 21, 36, 48–58], and their role in material removal processes [59–65]. Useful reviews are given by Lawn and co-workers [35, 66, 67]. Essentially similar arrays of cracks have also been produced in silicate glasses [68–82], various minerals [78], LiF [83–88], NaCl [84], MgO [83, 85, 87–91], ZnS [82, 91, 92], MgF_2 [91, 93], Si_3N_4 [91, 93], Al_2O_3 [93], $MgAl_2O_4$ [91], ZrO_2 [82, 94] and WC–Co cermets [91] by the impact (usually at normal incidence) of solid particles at velocities in the range $\sim 10^2$ to 10^3 m sec^{-1}. Moreover, just as in the case of static indentation, there have been a variety of attempts [30, 82, 91, 92, 95, 96] to use fracture mechanics to explain the propagation of these cracks and their role in material removal processes. In addition, a few studies [97–99] have been made of the flow processes occurring immediately below the impacting particle.

Two conclusions relevant to the erosion of ceramics by solid particle impact at normal incidence have emerged from these single contact studies. One is that the primary determinants of such erosion under fixed erosive conditions (i.e. when the size, density, shape, material and velocity of the impacting particle are held constant) are the dynamic hardness and the dynamic fracture toughness of the target. The former determines the target resistance to the plastic flow processes necessary to nucleate cracks in and around the region of contact, while the latter controls the growth of such cracks. The other conclusion is that the removal of material from pristine surfaces results primarily from the propagation of the lateral cracks rather than from the deeper-penetrating median and/or cone cracks. On heavily eroded surfaces, however, material removal is clearly a more complex process, because it is also influenced by interactions between cracks formed at adjacent impact sites. This is one reason why it is difficult to predict the erosion of ceramic materials from the results of single impact studies. Another is that the mass losses produced by impacts of irregularly-shaped particles can vary 1000-fold from one impact to another, depending on particle shape and orientation at impact [100].

Consequently, the few attempts [31, 91, 95, 96, 101] that have been made to predict erosion rates from single particle elastic–plastic impact damage mechanics have mostly been dimensional analyses restricted to the case of normal incidence and designed to rationalize the intuitively obvious experimental observation that erosion decreases with increasing target hardness and fracture toughness under these conditions. It should also be recognized that the hardness and fracture toughness values used in conjunction with these analyses were for the most part obtained from room-temperature tests performed on macroscopic specimens under static or near-static conditions. The individual impact events that cause erosion, however, typically involve deformation processes driven by transient loads that act for a few microseconds over areas having linear dimensions ~ 1 to $100\,\mu$m; and it is not clear how much hardness and fracture toughness are affected by the high strain rates, adiabatic heating and large compressive stresses characteristic of such events. Nor is it clear for ceramics of complex microstructure just how much hardness and fracture toughness can vary from one randomly selected impact site to another.

At its present level of sophistication, therefore, mathematical modelling of the erosion of ceramics by solid particle impact provides little or no information on such topics as the inception and evolution of mass loss from pristine surfaces, the variation of mass loss with impact angle, the relation between mass loss and microstructure, and the conditions under which melting might occur in the contact region. Neither are the currently available experimental data entirely unequivocal about these questions. For example, the existence of "incubation" phenomena in the early stages of erosion on pristine surfaces has been observed in SiC [102], but not in MgF_2 [100]. (Incubation effects occur also in borosilicate glass under elastic impact conditions [103], and a theory has been proposed to explain them [104, 105].) Furthermore, changing the erosive particle size relative to some characteristic microstructural dimension has been reported to change the appearance of the eroded surface of SiC with-

out altering the slope of the plot of erosion against particle size [102], but to produce quite different variations of mass loss with impact angle for different refractory concretes [106]. Significant, but as yet unexplained, effects of microstructure are also apparent in the different dependencies of mass loss on particle size and impact velocity observed in hot-pressed and reaction-bonded Si_3N_4, glass-bonded Al_2O_3 and hot-pressed MgF_2 [93]. Indirect evidence for the occurrence of melting during impact continues to accumulate from studies on alumina and mullite refractories [107], Al_2O_3 and silicate glasses [108], and metallic glasses [109].

In the absence of appropriate dynamic hardness and dynamic fracture toughness data, mathematical modelling of impact also fails to predict whether erosion should increase or decrease with increasing temperature, although it does suggest that this would be determined by the competing effects of a weak dependence of mass loss on dynamic hardness, which is expected to decrease markedly with increasing temperature, and a stronger dependence on dynamic fracture toughness, which probably increases but slowly with increasing temperature [101]. Therefore, it is not surprising to find that raising the temperature from 25 to 1000° C increases the erosion of hot-pressed Al_2O_3 and Si_3N_4 [110], sintered Al_2O_3 [110] and calcium aluminate-bonded Al_2O_3 [111] at shallow impact angles (where plastic flow plays its most important role in the material removal process [110]), but has no significant effect at normal incidence.

The present work attempts to answer some of the questions raised in the preceding paragraphs by studying erosion in the elastic–plastic impact regime under the simplest possible conditions: normal impingement of identical, rigid, spherical particles against a fine-grained, almost fully dense, single-phase ceramic at room temperature. Under such conditions the individual impact event was sufficiently reproducible that it was possible to resolve the incubation phenomena associated with the early stages of erosion. Moreover, the simple shape of the impacting particle permitted its equation of motion to be solved analytically to obtain the dynamic hardness from the dimensions of the impact crater. An additional simplifying factor was that all of the erosive particles used were large enough to ensure that the impact crater was always very much larger than the grain size.

2. Experimental methods and materials

The erosion experiments were carried out using a rotating arm apparatus described in a previous paper [112]. This apparatus consists of a steel tank which can be evacuated to ~1 Torr and houses a counter-balanced, tubular Al alloy arm that is rotated through a free-falling stream of erosive particles by an externally mounted, variable-speed electric motor. The specimens consisted of 6 mm thick, 16.5 mm diameter discs of MgO, the edges of which were protected by an annular Al alloy cover containing a central aperture of diameter 12.5 mm. Each disc was cemented to the end of a 12.5 mm diameter, 9 mm long cylinder of Al alloy, which in turn fitted into a recess in the end of the rotor arm.

Because this specimen configuration differed slightly from that used previously [112], it was necessary to recalibrate the apparatus to determine the ratio of the number of impacts, N_i, against the MgO specimen to the number of particles, N_p, introduced. This was done by counting the numbers of craters produced on pristine specimens when known numbers of particles were introduced at each of several different speeds of rotation. Since impacts could not occur at the periphery of the exposed area due to the 2 mm high raised rim of the cover, the effective specimen radius was taken to be $(R-r)$, where R is the radius of the aperture and r is the particle radius. Then, if the radius of the cross-section and the frequency of rotation of the arm are A and f, respectively, if the vertical velocity and the width of the stream of falling particles are u and $2R$, respectively, and if both the stream of particles and the specimen/rotor arm assembly are assumed to be of negligible dimensions in the direction of specimen travel, it can be shown that

$$\frac{N_i}{N_p} = \frac{\pi f(R-r)^2}{2Ru} \tag{1}$$

if $f \leqslant u/2(A+R-r)$, and that

$$\frac{N_i}{N_p} = \frac{f(R-r)^2(\pi - \theta + \frac{1}{2}\sin 2\theta)}{2Ru} \tag{2}$$

if $f \geqslant u/2(A+R-r)$, where

$$\theta = \cos^{-1}\left[\frac{(u/f)-2A}{2(R-r)}\right].$$

Fig. 1 shows experimental values of N_i/N_p determined as described above with 1.58 mm diameter WC–6 wt% Co spheres falling at a (photographi-

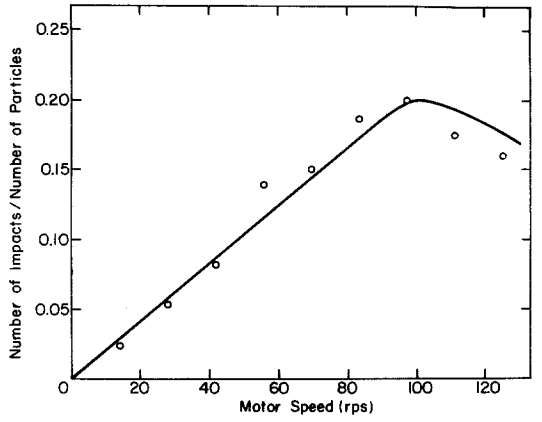

Figure 1 Ratio of number of impacts to number of spheres entering the apparatus plotted against motor speed.

TABLE I Result of an emission spectrographic analysis of the impurity content of the target material

Element	Concentration (ppm)
Si	500
Al	100
Fe	300
Mn	10
Ca	200
Ag	5
Cu	2

Not detected: B, Cr, Ni, Ti, Be, Na, Mo, Zr, Co, Zn, Sn, Ge, In, Bi, Ga, Pb, Sb, Y, Yb, Ba, Sr, La

cally determined) average velocity of $\sim 3\,\mathrm{m\,sec^{-1}}$. The line drawn through these data points represents the theoretical prediction of Equations 1 and 2 multiplied by an empirical correction factor of 0.82 to allow for the approximations involved in their derivation.

The MgO specimens used in this study were all cut from the same 6 mm thick sheet of hot-pressed polycrystalline material*. This had a translucent appearance, a grain size of $\sim 10\,\mu\mathrm{m}$, a density of 99.5% of that of an MgO monocrystal, and the impurity content listed in Table I. All experiments were performed on the as-received surface.

Each specimen was eroded incrementally at some fixed impact velocity in the range 10 to 90 $\mathrm{m\,sec^{-1}}$, and was weighed with a precision of $\pm 10\,\mu\mathrm{g}$ after each increment. Specimens were also rotated through 90° about the impact direction each time they were replaced in the apparatus in an attempt to cancel out the effects of the slight horizontal velocity gradient and vertical particle concentration gradient existing across the surface being eroded. The erosive particles were WC–6 wt% Co spheres with a density of $1.5 \times 10^4\,\mathrm{kg\,m^{-3}}$ and a Vickers hardness number of $\sim 2000\,\mathrm{kg\,mm^{-2}}$. Those used in the majority of experiments had a diameter of 1.58 ± 0.03 mm and weighed 30 ± 1 mg. However, in order to investigate the effect of particle size, a few experiments were also performed with spheres of diameters of 1.14 ± 0.02 mm and 0.35 ± 0.10 mm, which weighed 11.5 ± 0.5 mg and 0.10 to 0.60 mg, respectively. These spheres did not deform plastically on impact with the target, and only rarely fractured. Nor was evidence found of spheres or fragments of spheres embedded in the eroded surfaces.

3. Theoretical considerations

Provided that the elastic contribution to the total deformation is small, the impingement at normal incidence of a hard sphere against a plastically deforming target that exhibits negligible work-hardening may conveniently be described by assuming that the pressure over the area of contact is uniform and has a constant value p (the dynamic hardness) [113, 114]. Solving the resultant equation of motion yields [89]

$$pV = \tfrac{1}{2}mv_0^2, \tag{3}$$

where V is the crater volume, m is the mass of the sphere and v_0 is its initial impact velocity. A value of p can thus be found by measuring the crater diameter, d, and calculating the volume as that of a spherical cap having the same radius, r, as the sphere.

An approximate allowance for the effect of work-hardening can be incorporated into the model if it is assumed that Meyer's Law [115] applies under dynamic as well as static conditions, i.e. that

$$p = k\,d^{n-2}, \tag{4}$$

where k and n (the Meyer index) are constants. Solution of the corresponding equation of motion gives

$$p \simeq \left(\frac{n+2}{4}\right)\frac{mv_0^2}{2V} \tag{5}$$

at the end of the impact [113]. This expression is similar in form to Equation 3, which therefore

* Kindly supplied by Dr T. Vasilos of Avco Corporation, Waltham, Massachusetts, USA.

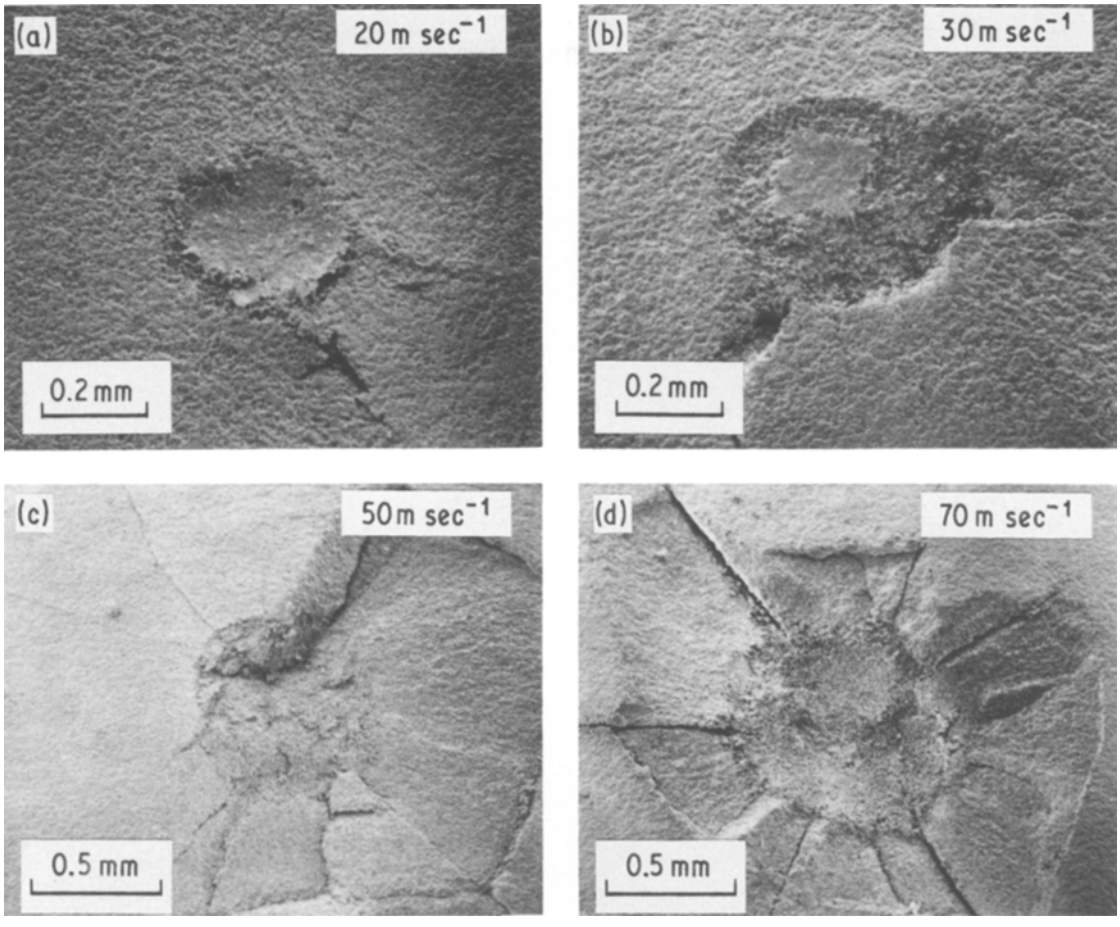

Figure 2 Damage due to single impacts of 1.58 mm diameter spheres as different velocities.

can be applied even when work-hardening occurs provided that it is remembered that the value of the terminal dynamic hardness obtained thereby is underestimated by a factor $(n + 2)/4$.

4. Results

Fig. 2. shows the damage produced by single, normal impacts of the 1.58 mm diameter spheres against as-received target surfaces. The crater produced at the lowest impact velocity (20 m sec^{-1}, Fig. 2a) has a relatively smooth interior and, although it is surrounded by a few short radial or median cracks, exhibits little evidence of material removal, except perhaps from its rim. As the impact velocity increases, however, material first spalls away from the interior surface of the crater in small quantities, Fig. 2b, and then flakes off in larger quantities from the region surrounding the crater as a result of the intersection of radial or median cracks with subsurface lateral cracks. Fig. 2c and d.

Owing to this loss of material from the periphery of the crater at higher impact velocities, accurate dynamic hardness values could only be measured for velocities $\lesssim 25$ m sec^{-1}. The two values obtained are shown in Fig. 3, together with static Meyer hardness* values obtained by indenting the as-received surface with similar spheres at loads ranging from ~ 50 to 600 N. The similar Meyer indices in the two cases (static, 2.57; dynamic, 2.6) suggest that the work-hardening behaviour of the target is little affected by strain rate.

Typical areas of the surfaces of specimens that have been eroded until the average amount of material removed per impact reached a constant value are shown in Fig. 4. In comparison with the single impact damage, the change in appearance with impact velocity is less striking. In every case

* The Meyer hardness is defined as the load divided by the area obtained by projecting the actual area of contact onto the original, undeformed surface.

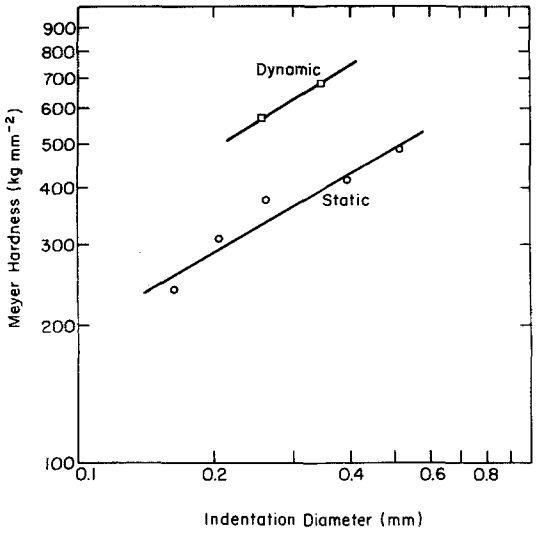

Figure 3 Variation of static (Meyer) and dynamic hardness with diameter of the crater produced by a 1.58 mm diameter sphere.

the eroded surface has an uneven topography made up of remnants of semi-obliterated impact craters, fracture surfaces created by lateral cracking and radial and/or median fractures. The scale of each of these features increases with increasing impact velocity, but the major mechanism of material removal appears in all cases to be the detachment from the exposed target surface of flakes formed by intersection of lateral cracks with the free surface and with radial and/or median cracks.

Details of individual impact sites on heavily eroded surfaces are shown in Fig. 5. In Fig, 5a a magnified view of the crater seen at lower centre in Fig. 4a reveals that about half of the original impression remains standing proud of the fracture surfaces exposed by the lateral cracks nucleated beneath it. The still higher magnification micrograph presented in Fig. 5b shows that the smooth interior of this crater consists of a thin layer of extremely heavily plastically deformed grains of MgO. Interesting features are that this layer is only

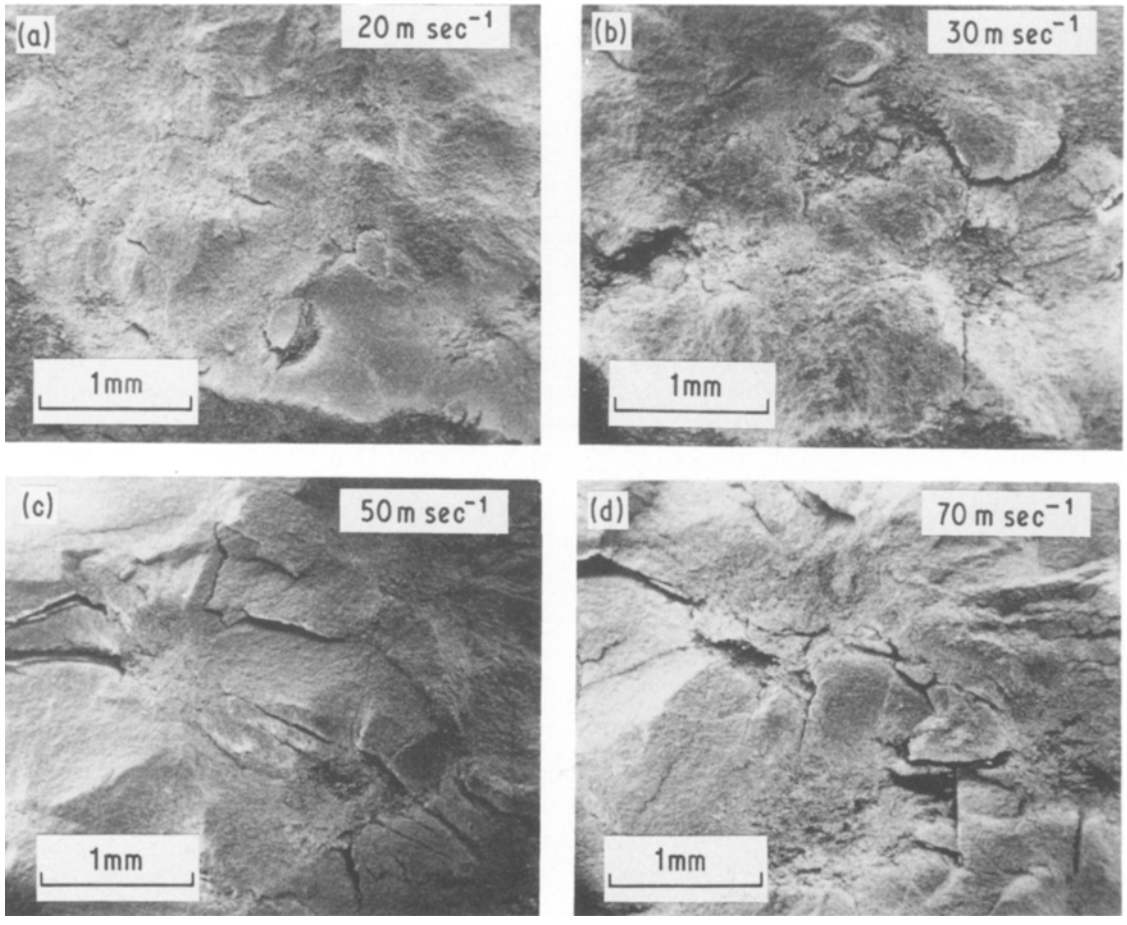

Figure 4 Steady-state erosion damage produced by 1.58 mm diameter spheres impacting at different velocities.

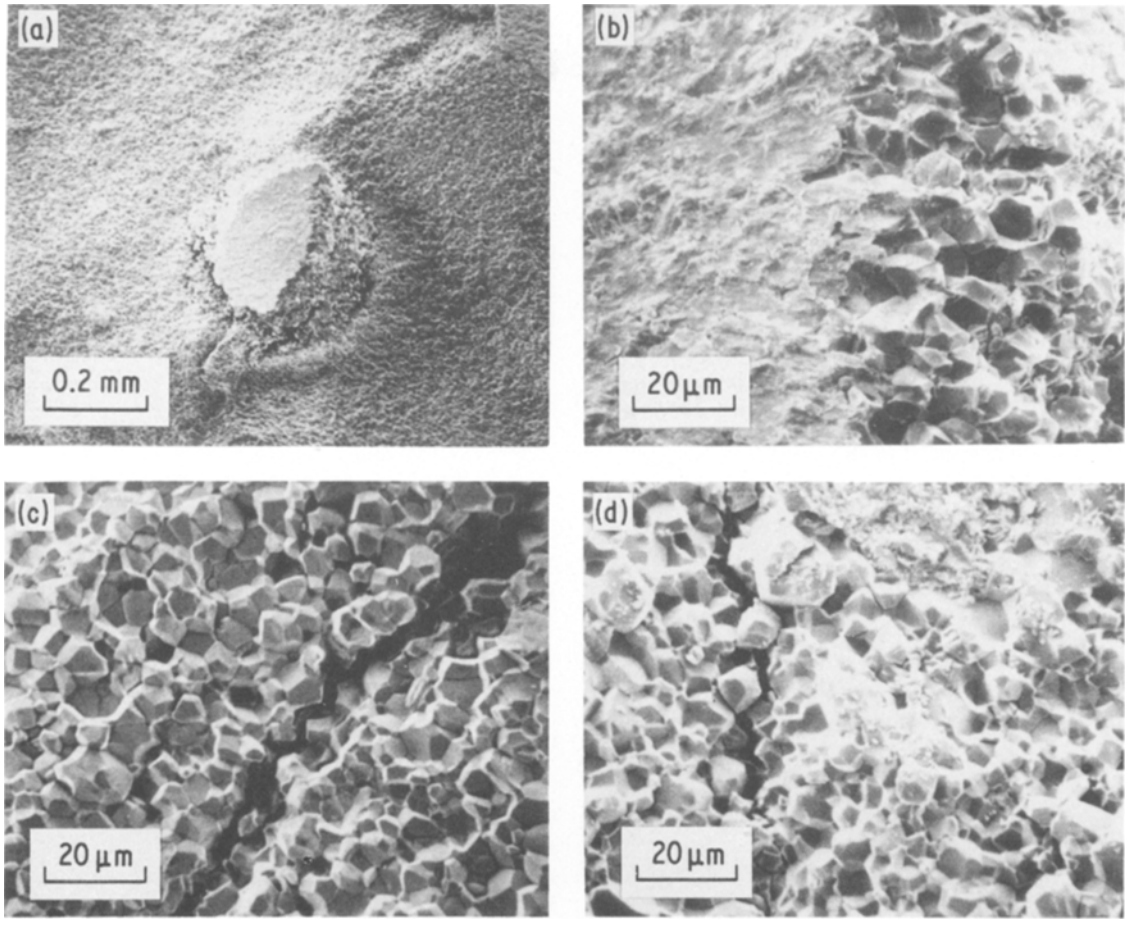

Figure 5 Details of the steady-state erosion damage produced by 1.58 mm diameter spheres impacting at 20 m sec^{-1} (a and b) and 70 m sec^{-1} (c and d).

one or two grain diameters thick and that the underlying material exposed at its edge exhibits both transgranular and intergranular fractures, but little evidence of gross plastic deformation. Fig. 5c and d are high magnification micrographs of regions situated respectively outside and inside a partly obliterated impact crater on a surface that had been heavily eroded at a velocity of 70 m sec^{-1}. The former, which shows a fracture surface formed by lateral fracture and intersected by a radial or median crack, reveals that both cracks follow intergranular fracture paths. The latter shows both another intergranular radial or median crack and the combination of intergranular and transgranular failure that occurs immediately below the impacting particle. In this case much of the thin overlayer of heavily plastically deformed material that originally lined the crater has been removed by subsequent impacts, and the debris that remains is typically ~ 1 μm in size.

The mass loss data obtained using 1.58 mm diameter spheres are shown in Figs 6 to 8. At every velocity studied, there was an initial incubation period during which the average mass of material

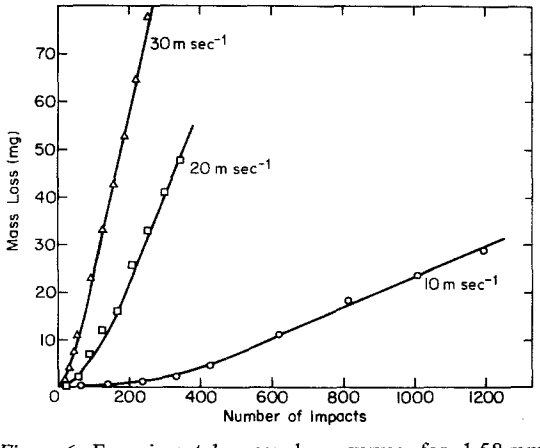

Figure 6 Experimental mass loss curves for 1.58 mm diameter spheres.

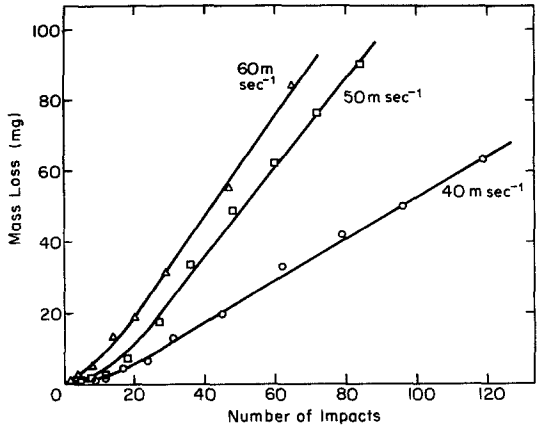

Figure 7 Experimental mass loss curves for 1.58 mm diameter spheres.

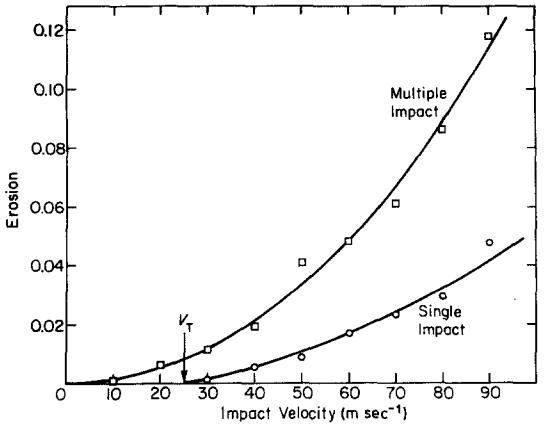

Figure 9 Erosion by 1.58 mm diameter spheres as a function of impact velocity under single and multiple impact conditions.

removed per impact increased with the number of impacts to some velocity-dependent steady-state value. Particularly at the higher impact velocities, Fig. 8, this incubation period was of very limited extent and would not have been observable had irregularly shaped erosive particles been employed. Power functions of the form

$$m_e = bN_i^{\beta}, \tag{6}$$

where m_e represents the mass loss due to erosion and b and β are constants for given erosive conditions, were fitted to the data in the incubation period at each impact velocity. The dimensionless erosion, E, which is defined by

$$E = \frac{1}{m}\frac{dm_e}{dN_i}, \tag{7}$$

was then calculated from the expression

$$E = \frac{b\beta}{m} N_i^{\beta-1}. \tag{8}$$

Fig. 9 compares the dependence of steady-state (linear) erosion on impact velocity, v_0, with the corresponding dependence of mass loss obtained from single, normal impacts of the same size spheres against as-received target surfaces. The curve fitted to the multiple impact data is of the form

$$E = av_0^{\alpha}, \tag{9}$$

where a is a constant and the velocity exponent $\alpha = 2.1$. However, the single impact data were found to be better represented by an equation of the form

$$E = a_1 (v_0^2 - v_T^2), \tag{10}$$

where a_1 is another constant and v_T is the threshold velocity (~ 25 m sec^{-1} in the present case) for detectable mass loss. Note that during steady-state erosion not only is the mass loss per impact at impact velocities greater than v_T roughly three times that produced by a similar impact against

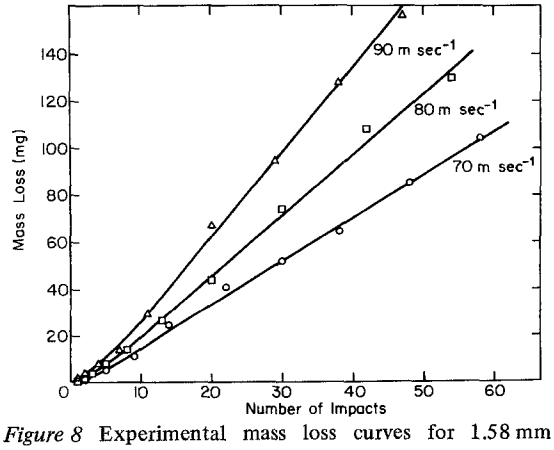

Figure 8 Experimental mass loss curves for 1.58 mm diameter spheres.

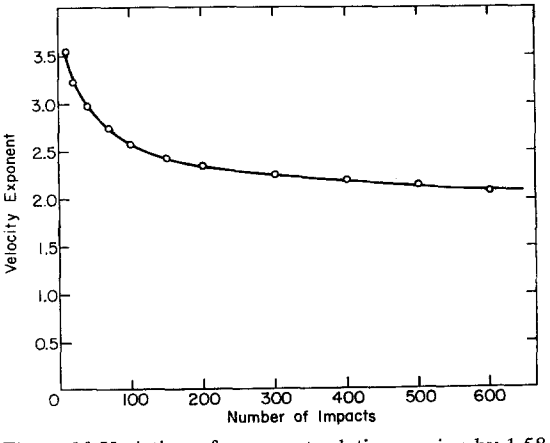

Figure 10 Variation of exponent relating erosion by 1.58 mm diameter spheres to impact velocity as a function of number of impacts.

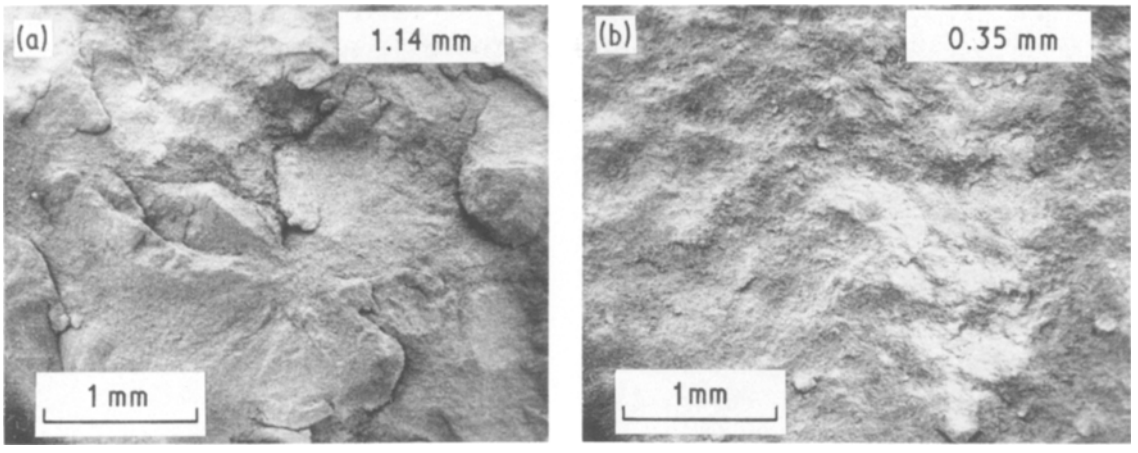

Figure 11 Steady-state erosion damage produced by different diameter spheres impacting at 50 m sec^{-1}.

the as-received surface, but also material is removed at velocities less than v_T, so that the effective threshold velocity tends towards zero as more and more impacts occur. In consequence, Equation 9 also becomes applicable to erosion during the incubation period, provided that sufficient impacts occur to produce measurable mass loss from all specimens. The variation with number of impacts of the velocity exponent α calculated in this fashion is shown in Fig. 10.

The change in the appearance of the steady-state eroded surface with decrease in erosive particle size at an impact velocity of 50 m sec^{-1} may be seen by comparing Figs 4c and 11. Essentially, the difference is one of scale rather than nature: all three sizes of particle produce the same characteristic combination of partly obliterated craters, lateral fracture surfaces and radial and/or median fractures. The corresponding mass loss data are plotted in Fig. 12 as functions of the mass rather than the number of particles impacting the target, and the values of the erosion calculated from the linear portions of these plots are presented in Fig. 13. These latter data show that under steady-state conditions the erosion of MgO by WC–6 wt% Co spheres depends on the particle diameter to the power 0.57.

5. Discussion

Single impacts of hard, millimeter-scale WC–6 wt% Co spheres against almost fully dense, fine-grained, polycrystalline MgO at normal incidence produce craters surrounded by the sort of array of radial and/or median and/or lateral cracks characteristic of impacts in which a significant amount of plastic deformation occurs beneath the particle. The interior of the crater is smooth and exhibits evidence of extensive plastic deformation. However, this plastic deformation extends only to a depth of one or two grain diameters (~ 10 to 20 μm), and crater formation is accommodated primarily by the residual strain generated in and around the region of contact as a result of crack-

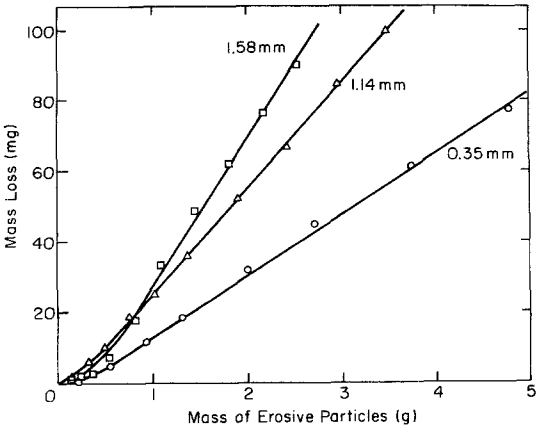

Figure 12 Experiemtal mass loss curves for different diameter spheres impacting at 50 m sec^{-1}.

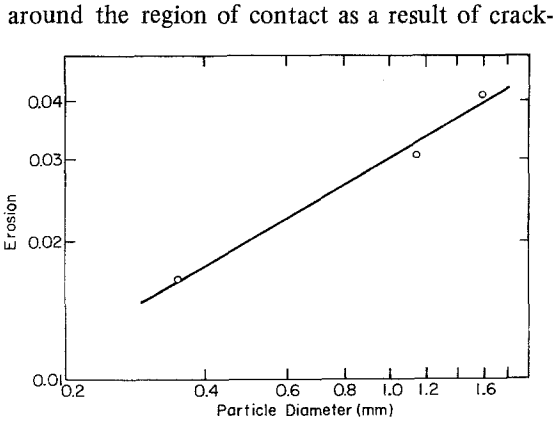

Figure 13 Variation of erosion in steady-state regime with sphere diameter at an impact velocity of 50 m sec^{-1}.

ing during the impact event. Immediately beneath the crater many short cracks are formed. Some are intergranular and others are transgranular, but none appear to extend for more than a few grain diameters. They are presumed to develop because they represent the easiest way for the individual grains of the target material, which has only two independent primary glide systems [116] and a very high critical resolved shear stress for secondary glide at or near room temperature [117], to accommodate the strain imposed by the impacting particle. In contrast, the radial, median and lateral cracks formed beyond the crater rim in response to the impact loading are few in number but extend over distances of a crater diameter or more. These latter cracks are all intergranular.

The important conclusion to be drawn from these observations is that it is not necessary to have extensive plastic flow (i.e. dislocation glide) in the contact region to produce radial and/or median and/or lateral cracking: microcracking, and probably any other irreversible mode of deformation capable of releasing strain energy, can produce the same pattern of fractures.

Mass losses large enough to be detected in the present experiments (i.e. $\gtrsim 10\,\mu g$) occurred at all impact velocities after a sufficient number of impacts, but only at velocities $\gtrsim 25\,m\,sec^{-1}$ for single impacts against as-received surfaces. Invariably, the dominant mechanism of material removal was detachment from the target surface of flakes formed by intersection of lateral cracks with the free surface and with radial and/or median cracks. Interaction between cracks formed at adjacent impact sites and repeated stressing of existing cracks by subsequent impacts both appeared to play an important role in this flaking process, because the average mass loss per impact during steady-state erosion at any impact velocity $\gtrsim 25$ $m\,sec^{-1}$ was about three times that produced by a similar velocity impact against the as-received target surface. The same processes also appear to be responsible for the absence of any threshold velocity for the occurrence of mass loss under multiple impact conditions. A secondary source of mass loss was spalling-away of the heavily plastically deformed material lining the impact craters, some of which material could occasionally be found adhering to the spent erosive spheres. Such spalling accounted for only a small fraction of the total mass loss, but is noted here because it does not appear to have been reported in other studies of the erosion of ceramics. No evidence was seen of melting in the impact zone.

An important result of the present studies is that they show quite unambiguously that the erosion of ceramics exhibits an incubation phase when the starting surface is not too heavily damaged. The existence of an incubation effect is implied by the three-fold increase in average mass loss per impact observed to accompany the change-over from initial to steady-state erosion conditions, and is demonstrated explicitly by the shape of the mass loss curves presented in Figs 6 to 8 and 12. These latter curves also make clear why there is controversy in the literature on this point [100, 102]: the incubation period is so short that it would be virtually impossible to document by means of an experiment employing irregular erosive particles which can give rise to orders of magnitude variations in the mass loss they produce per impact. Indeed, comparison of the present mass loss curves with those obtained for polycrystalline Al under identical erosive conditions [112], shows that the incubation period for the metal is ~ 100 times that for the ceramic. The reason for this is two-fold: first, because extensive cracking occurs around the impact craters in MgO, the area of the target affected by each impact is much greater than in the case of Al; and second, the flaking process primarily responsible for material removal from MgO can occur during individual impacts, whereas the process of platelet formation responsible for mass loss during the erosion of Al at normal incidence requires overlapping impacts. One noteworthy consequence of this difference in mechanism is that, even under steady-state erosion conditions, material removal from MgO must take place primarily from non-work-hardened surfaces.

Because the impact crater did not remain intact for impacts at velocities $\gtrsim 25\,m\,sec^{-1}$, only two dynamic hardness values were obtained from the present study, Fig. 3. These values are consistent with a Meyer index of 2.6, and suggest that the target work-hardens rapidly beneath the impacting particle. In contrast, previous studies [85, 87–90] of the normal impact of similar 1.58 mm diameter spheres against variously polished {1 0 0}, {1 1 0} and {1 1 1} surfaces of MgO single crystals showed the dynamic hardness to be independent of crater diameter in every case, implying a complete lack of work-hardening and a Meyer index of two. Likewise, there is a marked difference between

the responses of these same materials to static indentation by the same kind of spheres: the polycrystalline material exhibits a Meyer index of 2.57, indicative of rapid work-hardening, and {1 0 0}, {1 1 0} and {1 1 1} orientated single crystals exhibit Meyer indices ranging from 1.59 to 1.73 [118], implying work-softening. Correspondingly, the ratio of the dynamic to the static hardness, which has a value of ~ 2 and is independent of crater diameter in the case of the polycrystalline material, rises with increasing crater diameter from ~ 3 to 6 for single-crystal surfaces, depending on orientation.

The use in the preceding paragraph of the term work-hardening, with its implication of dislocation–dislocation interactions leading to a steady increase in yield stress as more and more strain accumulates, is not strictly correct; neither is the use of the term work-softening. The reason is that in none of the experiments discussed is either the static (Meyer) hardness or the dynamic hardness a true measure of the stress to produce dislocation motion. Rather, each parameter is used as a convenient representation of the total force required to operate all of the inter-related flow and fracture processes occurring in and around the region of contact. However, while it seems reasonably certain that most of the fracture occurring around impact craters and indentations in MgO is initiated by dislocation interactions, it is not clear how the stress required to produce these interactions (i.e. the hardness) depends on such microstructure-sensitive parameters as slip-line length, slip-line spacing, dislocation density, etc. Nor is it clear by how much the increase in fracture toughness associated with the change over from {1 0 0} and/or {1 1 0} cleavage in a single-crystal to to intergranular fracture in the present polycrystalline material effects the elastic stresses that constrain deformation in the region of contact under either static or dynamic conditions. At the present time, therefore, no detailed explanation of these data is possible. It is interesting to note, however, that such seamingly similar materials as MgO, LiF and NaCl all differ appreciably in the way in which their hardness varies with strain rate [84–90, 118], as do Ni and Al [87, 112, 118, 119]. Evidently there exists no simple way of relating dynamic hardness and dynamic fracture toughness to microstructure.

Finally, it is noted that none of the theories of erosion in either the elastic or the elastic–plastic impact regime provides an adequate explanation of the observed dependence of erosion on either impact velocity (Fig. 10) or particle size (Fig. 13). In particular, since none of these theories has sufficient resolution to distinguish between the incubation and steady-state erosion regimes, each predicts a constant velocity exponent in the range 2.4 to 3.2 [101]. Yet under the conditions of the present study the velocity exponent decreased from ~ 3.5 to ~ 2.1 in the course of the incubation period. Similar behaviour has also been observed in polycrystalline Al, although the incubation period is much longer and the range of variation of the velocity exponent rather larger [112]. In the case of the particle size exponent, there is also a significant discrepancy between theory and experiment: theory predicts an exponent of 0.7 to 1.2 [101], but the present experiments yielded a value of 0.57. This discrepancy is also apparent in the value of 0.39 obtained by Sheldon and Finnie [6] for the erosion of polycrystalline MgO by spherical steel shot.

Acknowledgement

This work was supported by the US Army Research Office under Grant No. DAAG29–79–C–0104.

References

1. C. M. PREECE and N. H. MACMILLAN, *Ann. Rev. Mater. Sci.* 7 (1975) 95.
2. G. P. TILLY, in "Treatise on Materials Science and Technology: Wear" Vol. 13, edited by H. Herman and D. Scott (Academic Press, New York and London, 1979) p. 287.
3. I. FINNIE, *Wear* **3** (1960) 87.
4. I. FINNIE and H. OH, Proceedings of the 1st Congress of the International Society for Rock Mechanics, Laboratorio Nacional de Engenharia Civil, Lisbon, Portugal, 1966, Vol. 2 (Laboratorio Nacional de Engenharia Civil, Lisbon, Portugal, 1966) p. 99.
5. H. L. OH, K. P. L. OH, S. VAIDYANATHAN and I. FINNIE, National Bureau of Standards Special Publ. No. 348 (National Bureau of Standards, Gaithersburg, Maryland, 1972) p. 119.
6. G. L. SHELDON and I. FINNIE, *J. Eng. Ind.* **88** (1966) 393.
7. G. L. SHELDON, *J. Basic Eng.* **92** (1970) 619.
8. H. HERTZ, *J. Reine Angew. Math.* **92** (1881) 156.
9. G. M. HAMILTON and L. E. GOODMAN, *J. Appl. Mech.* **33** (1966) 371.
10. W. WEIBULL, *Ing. Veterskaps Akad. Handlings, Stockholm* **151** (1939) 1.
11. G. L. SHELDON and I. FINNIE, *J. Eng. Ind.* **88** (1966) 387.
12. H. UETZ and J. FÖHL, *Wear* **20** (1972) 299.
13. G. A. SARGENT, P. K. MEHROTRA and H. CONRAD, Proceedings of the 5th International

Conference on Erosion by Solid and Liquid Impact (Cavendish Laboratory, Cambridge, England, 1979) Paper No. 28.
14. C. J. STUDMAN and J. E. FIELD, *J. Phys. D* **9** (1976) 857.
15. S. PALMQUIST, *Jernkontorets Ann.* **141** (1957) 300.
16. *Idem, Arch. Eisenhüttenw.* **33** (1962) 29.
17. I. M. OGILVY, C. M. PERROTT and J. W. SUITER, *Wear* **43** (1977) 239.
18. H. E. EXNER, *Trans. AIME* **245** (1969) 677.
19. K. E. PUTTICK, *J. Phys. E.* **6** (1973) 116.
20. K. E. PUTTICK, L. S. A. SMITH and L. E. MILLER, *J. Phys. D* **10** (1977) 617.
21. K. E. PUTTICK, *ibid* **11** (1978) 595.
22. J. T. HAGAN and M. M. CHAUDHRI, *J. Mater. Sci.* **12** (1977) 1055.
23. R. K. BANERJEE and P. FELTHAM, *ibid* **9** (1974) 1478.
24. J. LANKFORD and D. L. DAVIDSON, *ibid* **9** (1979) 1662.
25. M. V. SWAIN, Ph.D Thesis, University of New South Wales, Australia (1973).
26. J. LANKFORD and D. L. DAVIDSON, *J. Mater. Sci.* **14** (1979) 1669.
27. B. J. HOCKEY and B. R. LAWN, *ibid.* **10** (1975) 1275.
28. M. G. S. NAYLOR and T. F. PAGE, Proceedings of the 5th International Conference on Erosion by Solid and Liquid Impact, (Cavendish Laboratory, Cambridge, England, 1979) Paper No. 32.
29. J. LANKFORD, "Fracture Mechanics of Ceramics", Vol. 3 (Plenum Press, New York, 1978) p. 245.
30. *Idem, Scripta Met.* **11** (1977) 349.
31. A. G. EVANS and T. R. WILSHAW, *Acta Met.* **24** (1976) 939.
32. M. V. SWAIN and B. R. LAWN, *Phys. Stat. Sol.* **35** (1969) 909.
33. J. PAONE and S. TANDANAND, *Trans. ASME* **235** (1966) 113.
34. M. V. SWAIN and B. R. LAWN, "Indentation Fracture in Brittle Rocks and Glasses", Tech. Rep. MML-TR-76-12C, Martin-Marietta Labs., Baltimore, Maryland (1976).
35. B. R. LAWN and T. R. WILSHAW, *J. Mater. Sci.* **10** (1975) 1049.
36. B. R. LAWN and M. V. SWAIN, *ibid* **10** (1975) 113.
37. M. V. SWAIN and J. T. HAGAN, *J. Phys. D* **9** (1976) 2201.
38. K. PHILLIPS, *J. Mater. Sci.* **11** (1976) 2354.
39. J. T. HAGAN and M. V. SWAIN, *J. Phys. D* **11** (1978) 2091.
40. K. W. PETER, *J. Non-Cryst. Solids* **5** (1970) 103.
41. K. PETER, *Glastech. Ber.* **37** (1964) 333.
42. E. DICK, *ibid* **43** (1970) 16.
43. M. V. SWAIN, *J. Amer. Ceram. Soc.* **62** (1979) 318.
44. J. T. HAGAN, *J. Mater. Sci.* **14** (1979) 462.
45. A. ARORA, D. B. MARSHALL and B. R. LAWN, *J. Non-Cryst. Solids* **31** (1979) 415.
46. B. R. LAWN and A. G. EVANS, *J. Mater. Sci.* **12** (1977) 2195.
47. J. T. HAGAN, *ibid* **14** (1979) 2975.
48. R. K. VISWANADHAM and J. D. VENABLES, *Met. Trans* **8A** (1977) 187.
49. C. M. PERROTT, *Wear* **45** (1977) 293.
50. *Idem, ibid* **47** (1978) 81.
51. B. R. LAWN, T. JENSEN and A. ARORA, *J. Mater. Sci.* **11** (1976) 573.
52. B. R. LAWN, M. V. SWAIN and K. PHILLIPS, *ibid* **10** (1975) 1236.
53. A. G. EVANS and E. A. CHARLES, *J. Amer. Ceram. Soc.* **59** (1976) 371.
54. M. G. MENDIRATTA and J. J. PETROVIC, *J. Mater. Sci.* **11** (1976) 973.
55. B. R. LAWN and D. B. MARSHALL, *J. Amer. Ceram. Soc.* **62** (1979) 347.
56. B. R. LAWN and E. R. FULLER, *J. Mater. Sci.* **10** (1975) 2016.
57. D. B. MARSHALL and B. R. LAWN, *ibid* **14** (1979) 2001.
58. M. V. SWAIN, *ibid* **11** (1976) 2345.
59. *Idem, Wear* **35** (1975) 185.
60. B. R. LAWN, *ibid* **33** (1975) 369.
61. M. V. SWAIN, *Proc. Roy. Soc. Lond.* **A366** (1979) 575.
62. K. E. PUTTICK, M. A. SHAHID and M. M. HOSSEINI, *J. Phys. D* **12** (1979) 195.
63. K. PETER and E. DICK, *Glastech. Ber.* **40** (1967) 470.
64. M. V. SWAIN, "Fracture Mechanics of Ceramics", Vol. 3 (Plenum Press, New York, 1978) p. 257.
65. J. D. B. VELDKAMP, N. HATTU and V. A. C. SNIJDERS, *ibid,* p. 273.
66. B. R. LAWN and D. B. MARSHALL, *ibid,* p. 205.
67. B. R. LAWN and T. R. WILSHAW, "Fracture of Brittle Solids" (Cambridge University Press, 1975).
68. J. P. A. TILLET, *Proc. Phys. Soc.* **B69** (1956) 47.
69. Y. M. TSAI and H. KOLSKY, *J. Mech. Phys. Solids* **15** (1967) 263.
70. G. P. CHEREPANOV and V. B. SOKOLINSKY, *Eng. Fract. Mech.* **4** (1972) 205.
71. C. G. KNIGHT, M. V. SWAIN and M. M. CHAUDHRI, *J. Mater. Sci.* **12** (1977) 1573.
72. M. M. CHAUDHRI and S. M. WALLEY, *Phil. Mag.* **37A** (1978) 153.
73. M. M. CHAUDHRI and P. A. BROPHY, *J. Mater. Sci.* **15** (1980) 345.
74. H. P. KIRCHNER and R. M. GRUVER, *Mater. Sci. Eng.* **28** (1977) 153.
75. *Idem, ibid* **33** (1978) 101.
76. M. M. CHAUDHRI, C. G. KNIGHT and M. V. SWAIN, Proceedings of the 12th International Congress on High Speed Photography, Society of Photo-Optical Instrumentation Engineers, Washington, D.C. (1977) p. 371.
77. J. F. VEDDER and J. -C. MANDEVILLE, *J. Geophys. Res.* **79** (1974) 3247.
78. J. F. VEDDER, *Earth Planet. Sci. Letters* **11** (1971) 291.
79. L. A. GLENN, *J. Mech. Phys. Solids* **24** (1976) 93.
80. M. M. CHAUDHRI and S. M. WALLEY, "Fracture Mechanics of Ceramics", Vol. 3 (Plenum Press, New York, 1978) p. 349.

81. H. P. KIRCHNER and R. M. GRUVER, *ibid,* p. 365.
82. D. M. RICHARD and H. P. KIRCHNER, Proceedings of the 5th International Conference on Eroratory, Cambridge, England (Cavendish Laboratory, Cambridge, 1979) Paper No. 27.
83. S. V. HOOKER, and W. F. ADLER, "Fracture Mechanics of Ceramics", Vol. 3 (Plenum Press, New York, 1978) p. 333.
84. M. M. CHAUDHRI and A. STEPHENS, Proceedings of the 13th International Conference on High Speed Photography and Photonics, Japanese Society of Precision Engineers, Tokyo, Japan (1979) p. 726.
85. B. N. PRAMILA BAI, MSc Thesis, The Pennsylvania State University, University Park, Pennsylvania (1978).
86. D. G. RICKERBY, B. N. PRAMILA BAI and N. H. MACMILLAN, *J. Mater. Sci.* **14** (1979) 3006.
87. D. G. ROCKERBY and N. H. MACMILLAN, Proceedings of the 5th International Conference on Erosion by Solid and Liquid Impact, Cavendish Laboratory, Cambridge, England (Cavendish Laboratory, Cambridge, 1979) Paper No. 29.
88. D. G. RICKERBY, B. N. PRAMILA BAI and N. H. MACMILLAN, "Energy and Ceramics" (Elsevier, Lausanne, Switzerland, 1980) p. 752.
89. *Idem, J. Mater. Sci.* **14** (1979) 1807.
90. D. G. RICKERBY and N. H. MACMILLAN, *ibid.* **15** (1980) 2435.
91. A. G. EVANS, M. E. GULDEN and M. ROSENBLATT, *Proc. Roy. Soc. Lond.* **A361** (1978) 343.
92. A. G. EVANS and T. R. WILSHAW, *J. Mater. Sci.* **12** (1977) 97.
93. M. E. GULDEN, ASTM Special Tech. Publ. No. 664, ASTM, Philadelphia (1979) p. 101.
94. H. P. KIRCHNER, R. M. GRUVER, D. M. RICHARD and R. C. GARVIE, *Mater. Sci. Eng.* **40** (1979) 49.
95. A. G. EVANS, "Fracture Mechanics of Ceramics", Vol. 3 (Plenum Press, New York, 1978) p. 303.
96. A. G. EVANS, in "Treatise on Materials Science and Technology: Erosion" Vol. 16, edited by H. Herman and C. M. Preece (Academic Press, New York and London, 1979) p. 1.
97. B. J. HOCKEY and S. M. WIEDERHORN. Proceedings of the 5th International Conference on Erosion by Solid and Liquid Impact, Cavandish Laboratory, Cambridge, England (Cavendish Laboratory, Cambridge, 1979) Paper No. 26.
98. J. NARAYAN and J. WASHBURN, *Wear* **23** (1973) 128.
99. J. NARAYAN, *ibid* **25** (1973) 99.
100. M. E. GULDEN, *J. Amer. Ceram. Soc.* **63** (1980) 121.
101. A. W. RUFF and S. M. WEIDERHORN, in "Treatise on Materials Science and Technology: Erosion" Vol. 16, edited by H. Herman and C. M. Preece (Academic Press, New York and London, 1979) p. 69.
102. J. L. ROUTBORT, R. O. SCATTERGOOD and A. P. L. TURNER, *Wear* **59** (1980) 363.
103. W. F. ADLER, *J. Non-Cryst. Solids* **19** (1975) 335.
104. *Idem, Wear* **37** (1976) 345.
105. *Idem, ibid.* **37** (1976) 353.
106. M. S. CROWLEY, *Ceram. Bull.* **48** (1969) 707.
107. C. S. YUST and R. S. CROUSE, *Wear* **51** (1978) 193.
108. B. R. LAWN, B. J. HOCKEY and S. M. WIEDERHORN, *J. Amer. Ceram. Soc.* **63** (1980) 356.
109. A. S. ARGON, private communication (1980).
110. B. J. HOCKEY, S. M. WIEDERHORN and H. JOHNSON, "Fracture Mechanics of Ceramics", Vol. 3 (Plenum Press, New York, 1978) p. 379.
111. S. M. WIEDERHORN and D. E. ROBERTS, *Ceram. Bull.* **55** (1976) 185.
112. D. G. RICKERBY and N. H. MACMILLAN, *Wear* **60** (1980) 369.
113. D. TABOR, "The Hardness of Metals" (Clarendon Press, Oxford, 1951) p. 47.
114. J. P. ANDREWS, *Phil. Mag.* **9** (1930) 593.
115. E. MEYER, *Z. Vereines Deutsch. Ing.* **52** (1908) 645, 740, 835.
116. G. W. GROVES and A. KELLY, *Phil. Mag,* **8** (1963) 877.
117. C. O. HULSE, S. M. COPLEY and J. A. PASK. *J Amer. Ceram. Soc.* **46** (1963) 317.
118. D. G. RICKERBY and N. H. MACMILLAN, *Mater. Sci. Eng.* **40** (1979) 251.
119. N. C. SINK, MSc Thesis, The Pennsylvania State University, University Park, Pennsylvania (1978).

Received 10 September and accepted 11 November 1980.